RSC Advances

PAPER

View Article Online
View Journal | View Issue

Cite this: *RSC Adv.*, 2025, **15**, 7897

Non-enzymatic dopamine detection using iron doped ZIF-8-based electrochemical sensor

Nugraha,*[ab] Nurul Hanifah,[a] Atqiya Muslihati,[a] Muhammad Fadlan Raihan,[a] Ni Luh Wulan Septiani *[c] and Brian Yuliarto[ab]

Dopamine plays a vital function in the central nervous, cardiovascular, and endocrine systems. The precise identification of dopamine is essential for the diagnosis and treatment of different disorders. Electrochemical approaches provide a hopeful substitute for intricate methods such as HPLC and mass spectroscopy. However, the presence of other interference from other substances is a challenge. Modifying the electrode surface or using Zeolitic Imidazolate Framework 8 (ZIF-8) coated with iron can enhance sensitivity and selectivity. Iron-modified ZIF-8 (Fe-ZIF-8) has shown excellent catalytic activity. This study proposes the development of Fe-ZIF-8 for dopamine detection using electrochemical methods. Fe-ZIF-8 displayed sensitive and selective performance, surpassing interfering compounds. A successful synthesis of Fe-ZIF-8 composites with varying iron ratios was achieved, with Fe5-ZIF-8 exhibiting the highest oxidation and reduction peaks. The performance of the Fe5-ZIF-8/GCE sensor was evaluated, demonstrating superior sensing performance in linear range of 0.05–20 μM. The limit of detection (LOD) was determined as 0.035 μM, falling within the concentration of dopamine in human serum. The sensor also exhibited selectivity towards interfering substances, including uric acid, ascorbic acid, and urea. These findings highlight the successful synthesis and promising performance of Fe5-ZIF-8 as a selective sensor material.

Received 5th May 2024
Accepted 10th December 2024

DOI: 10.1039/d4ra03307h

rsc.li/rsc-advances

1. Introduction

Dopamine is a vital neurotransmitter that has a crucial function in regulating the operational functions of the central nervous, cardiovascular, and endocrine systems.[1] When there are unusual levels of dopamine in the body, it has been connected to various illnesses like Alzheimer's disease, bipolar disorder, schizophrenia, and Parkinson's disease.[2,3] Hence, a sensitive and precise method of detecting dopamine is required for medical diagnosis and treatment purposes.

Various techniques are available to accurately and selectively detect dopamine, such as High-Performance Liquid Chromatography (HPLC), mass spectroscopy, and a combination of both methods.[4] However, these approaches can be complex, costly, time-consuming, and require skilled operators. To overcome these limitations, electrochemical techniques have been developed, enabling the detection of dopamine's electroactive performance with a simple procedure and more accessible.[5] The electrochemical techniques in the field of chemicals or biosensors are utilized to obtain signals in the form of electrical signals from the interaction between the electrode surface and the target analyte. This technique offers high sensitivity, low detection limits, ease of use, and requires only a small amount of analyte. Selective detection of specific targets is a major challenge in the use of electrochemical-based sensors. Therefore, the use of bioreceptors or nanomaterials as supporting materials is employed to enhance selectivity.[6–8] For example, the presence of interfering substances like uric acid and ascorbic acid can pose challenges due to their similar oxidation potential and higher concentrations compared to dopamine.[9,10] The use of nanomaterials as modifiers is a strategic choice for creating dopamine sensors with high selectivity, superior stability, and an easy modification process, where the use of proteins such as enzymes, which are susceptible to environmental changes, can be avoided. An example of such modification is coating the working electrode with Zeolitic Imidazolate Framework 8 (ZIF-8), which has been enhanced with iron (Fe) to enhance the sensitivity and selectivity of dopamine detection using electrochemical methods.

ZIF-8 is a specific type of zeolitic imidazolate framework (ZIF) composed of metallic zinc (Zn) and the organic linker 2-methylimidazole.[11] ZIF-8 possesses a porous structure and a large specific surface area, however ZIF-8 is reported to have low conductivity affecting their performance as chemical and biosensors.[12–14] Some works reported adding transition metal doping to ZIF-8 can enhance conductivity as well as catalytic

[a]*Advanced Functional Materials Laboratory, Faculty of Industrial Technology, Institut Teknologi Bandung, Bandung 40132, Indonesia. E-mail: nugraha@itb.ac.id*

[b]*Research Center for Nanosciences and Nanotechnology (RCNN), Institut Teknologi Bandung, Bandung 40132, Indonesia*

[c]*Research Center for Electronics, National Research and Innovation Agency (BRIN), Bandung 40135, Indonesia. E-mail: nilu010@brin.go.id*

activity.[15,16] Among the transition metals, studies have indicated that iron-modified ZIF-8 (Fe-ZIF-8) exhibits superior catalytic activity.[17,18] Fe-ZIF-8 has been extensively studied as a photocatalyst material, its application as an electrochemical sensor material remains unexplored.

In this study, developed ZIF-8 by modifying the synthesis process of ZIF-8 through the incorporation of metal ions, specifically iron (Fe) ions, to capitalize on its advantages. The addition of Fe in an optimal manner can significantly improve the electrochemical capabilities of the ZIF material. In our research, we successfully modified a glassy carbon electrode (GCE) by incorporating Fe-ZIF-8 nanomaterial into its working electrode. This modification allowed us to detect dopamine in neutral conditions using electrochemical techniques such as cyclic voltammetry (CV), differential pulse voltammetry (DPV), and chronoamperometry (CA). The Fe-ZIF-8 composite exhibited notable sensitivity and selectivity in detecting dopamine compared to various interfering compounds.

2. Experiment

2.1 Materials

Zinc nitrate hexahydrate ($Zn(NO_3)_2 \cdot 6H_2O$), iron(II) chloride tetrahydrate ($FeCl_2 \cdot 4H_2O$), and 2-methylimidazole (HmIM) 99% were purchased from Merck. While dopamine hydrochloride, urea, uric acid, and ascorbic acid were acquired from Sigma Aldrich. Without further purification, analytical-grade chemicals were used for all applications.

2.2 Synthesis of ZIF-8 and Fe-ZIF-8

The ZIF-8 was synthesized using a precipitation method described by,[19] but with a modification involving the combination of HmIM as a ligand and Zn^{2+} and Fe^{2+} ions as metal center in a 1 : 4 ratio. The percentage of Fe^{2+} was varied to 0%, 1%, 3%, 5%, 7%, and 10% while maintaining a total concentration of 5 mmol. To prepare the solution, 1.642 g (20 mmol) of HmIM was dissolved in 100 mL of methanol and stirred at room temperature for 5 minutes. Next, the HmIM solution was gently added to the Zn^{2+} and Fe^{2+} solution and stirred for 2 hours at room temperature. The resulting mixture was incubated for 24 hours at room temperature. To purify the product, the precipitate was washed multiple times using methanol. Finally, the precipitate was dried overnight at 60 °C. All the samples are labelled to Fe0-ZIF-8, Fe1-ZIF-8, Fe3-ZIF-8, Fe5-ZIF-8, Fe7-ZIF-8, and Fe10-ZIF-8 for each additional of 0%, 1%, 3%, 5%, 7%, and 10% of Fe respectively.

2.3 Structural characterization

The physicochemical properties of Fe-ZIF-8 were analyzed using three techniques: X-ray diffraction (XRD), surface and pore analyzer, and Scanning Electron Microscope (SEM). XRD was utilized to assess the material's crystallinity. Surface and pore analyzer provided information on the specific surface area, porosity, and the material's adsorption–desorption profile. SEM was employed to examine the morphological structure of the material.

2.4 Dopamine sensor performance test

To prepare the sensing electrode, 1.5 mg of the ZIF-8 powder was dispersed in 980 μL of distilled water using a bath sonicator for 15 minutes until a homogeneous suspension was obtained. Then, 20 μL of 5% Nafion solution was added and sonicated again for 15 minutes. Next, 6 μL of the suspension was drop-casted onto the glassy carbon electrode (GCE) surface as the working electrode (WE) and dried at room temperature.

The sensor performance test involved electrochemical measurements techniques, specifically cyclic voltammetry (CV), differential pulse voltammetry (DPV), and chronoamperometry (CA). For these measurements, three electrodes were used: an Ag/AgCl reference electrode (RE), a platinum wire counter electrode (CE), and GCE modified with the optimum material as the WE. The test was performed in a dopamine solution in phosphate-buffered saline (PBS) with a concentration of 0.01 M and a pH of 7.4.

CV measurements were conducted within a voltage range of −0.6 V to 0.6 V using different scan rates (25–200 mV s^{-1}) to determine the charge transfer mechanism at the electrode surface. DPV measurements were performed to analyze the response of dopamine concentrations ranging from 0.05 μM to 20 μM. The DPV parameters used were a potential range of −0.05 V to 0.3 V, an amplitude of 50 mV, a step height of 4 mV, a pulse width of 0.2 seconds, a step width of 0.5 seconds, and a sampling period of 0.01667 seconds. The current response profile was then analyzed to determine the sensor's sensitivity and limit of detection.

CA measurements were conducted to assess the selectivity of the sensor. The measurements were performed at a constant potential of 0.1 V in a stirred solution while observing changes in current caused by potential interferences such as uric acid, ascorbic acid, and urea. The tests were carried out on the GCE modified with the optimum material measurements were performed on mixed analytes solutions containing 10 mM urea, 1 mM ascorbic acid, 1 mM uric acid, and 0.1 mM dopamine.

3. Result and discussions

The proposed non-enzymatic dopamine sensor was designed based on Fe-ZIF-8/GCE. The distinctive structure of Fe-ZIF-8 was obtained using the precipitation method, as mentioned in the methods section. The Fe-ZIF-8 material was utilized as the sensing material and deposited onto a GCE through a casting procedure. As the structure of the material, the XRD diffraction shows that the Fe-ZIF-8 has high crystallinity. The XRD peaks at 2θ of 7.34°, 10.45°, 12.78°, 14.75°, 16.50°, and 18.07° are originated from plane of (011), (002), (112), (022), (013), and (222) respectively. The XRD pattern shows a topology with the SOD type which indicates that iron has succeeded in replacing zinc in ZIF-8 (see in Fig. 1) [20] The resulting Fe modified ZIF-8 is also pure because no additional peaks from other phases. Additionally, the XRD peak was in good agreement with the reported XRD pattern in previous research conducted by.[21] Additionally, there is an increase in peak intensity as the Fe concentration

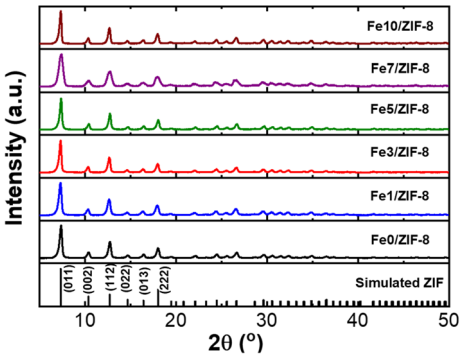

Fig. 1 XRD pattern simulated ZIF-8 and synthesized Fe-ZIF 8.

increases, this means that the iron can induce the crystal growth of ZIF-8.

The SEM results revealed that the shape of ZIF-8 remained unaffected by an increase in the iron content. All samples exhibited a rhombic dodecahedron which is the most stable shape for ZIF-8 (see in Fig. 2).[22,23] In addition, the addition of Fe did not affect the particle shape revealing the successful incorporation of Fe in ZIF-8 matrix. As observed, incorporating an iron up to 5% did not alter the size of the ZIF-8 structure, which exhibited a uniform size of approximately 90 nm. Conversely, when the added ratio exceeded 5%, there was a significant increase in particle size. Different in valence state of Zn and Fe induces the creation of vacancy defect to keep the charge balancing. The defect might increase the rate of particle growth resulting in bigger particle size.[23,24]

To confirm the successful of Fe incorporated in ZIF-8, EDX analysis has been performed for Fe5-ZIF-8. As seen in Fig. 3, all the main elements which are carbon, nitrogen, Zn, and Fe are well distributed in the particles. This result strengthens the XRD patterns where all Fe modified ZIF-8 show similar diffraction patterns with the pure ZIF-8 one. This phenomenon indicates that Fe elements are successfully inserted into the ZIF-8 crystal host by substituting mechanism.

By performing a CV scan in the potential range of −0.6–0.6 V, the optimum material for detecting dopamine was determined. The solution used for the profiling contained 0.1 mM of dopamine in PBS (0.01 M, pH 7.4). Fig. 4a depicts the voltammogram of all samples, compared to bare GCE, all the Fe modified ZIF-8 samples demonstrate higher oxidation and reduction current revealing that zinc metal center is clearly active. Additionally, the presence of Fe also improves the catalytic activity of ZIF-8. In

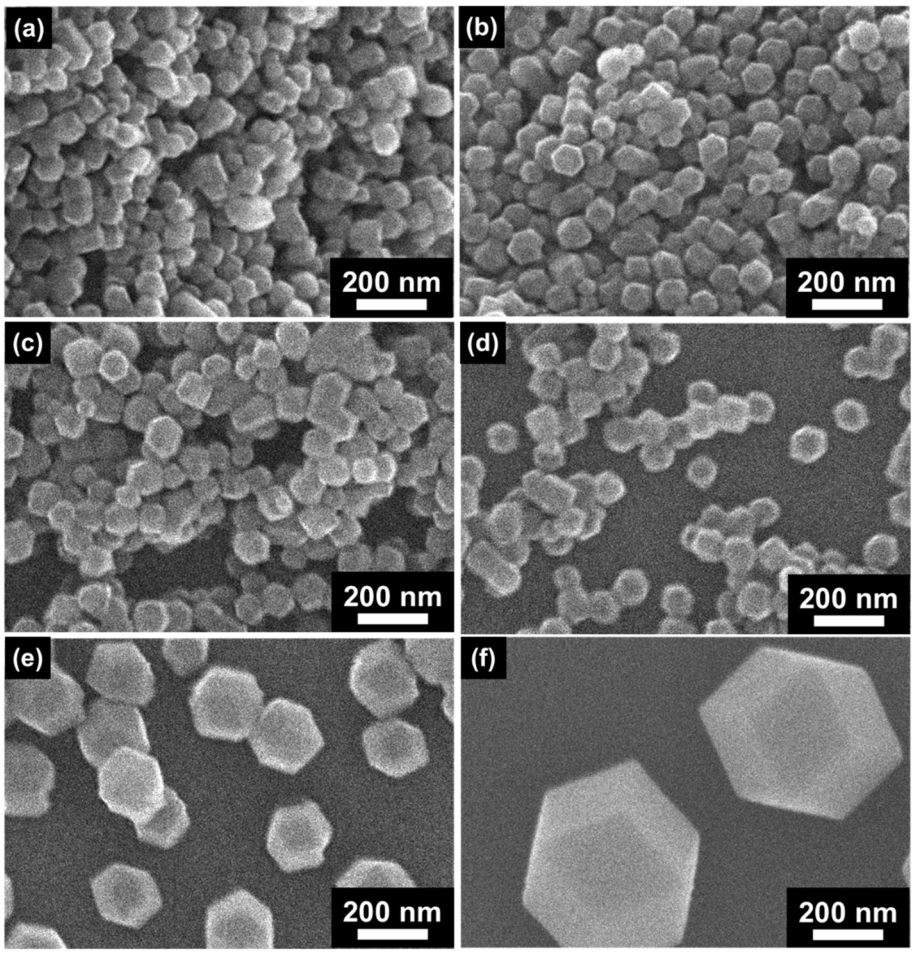

Fig. 2 SEM images of (a) Fe0-ZIF-8, (b) Fe1-ZIF-8, (c) Fe3-ZIF-8, (d) Fe5-ZIF-8, (e) Fe7-ZIF-8, (f) Fe10-ZIF-8.

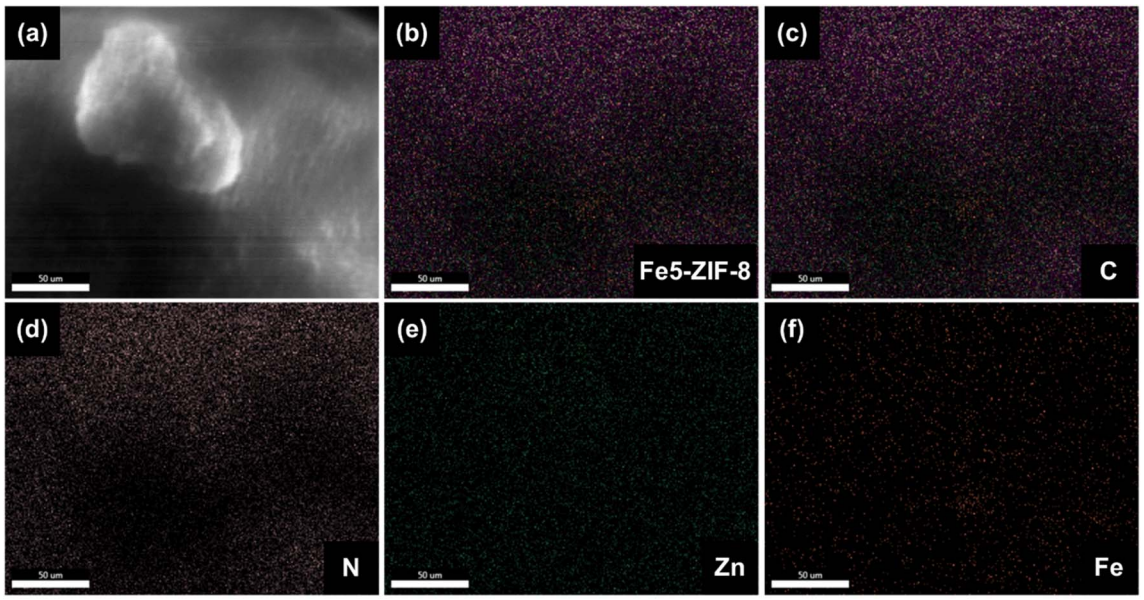

Fig. 3 EDX analysis of (a and b) Fe5-ZIF-8 confirming the distribution of (c) C, (d) N, (e) Zn, and (f) Fe.

this case Fe enrich the oxidation state variation and improve the conductivity of ZIF-8. Fig. 4a clearly demonstrates that the modified Fe5-ZIF-8/GCE outperformed other modifications, in terms of oxidation–reduction peaks. Notably, there was no significant difference in response among modifications with different ratios, except for ratios above 5% which exhibited a decrease in the current response. Based on the CV scan results, it was concluded that the ideal material for detecting dopamine was an iron ratio of 5% (Fe5-ZIF-8). The highest performance of Fe5-ZIF-8 is also supported by its high surface area. As shown in Fig. 5, all samples show similar profiles where there is no significant difference in surface area. Using BET technique, the specific surface area for each Fe0/ZIF-8, Fe1/ZIF-8, Fe3/ZIF-8, Fe5/ZIF-8, Fe7/ZIF-8, and Fe10/ZIF-8 is 1630 $cm^2\ g^{-1}$ 1618 $cm^2\ g^{-1}$, 1631 $cm^2\ g^{-1}$, 1622 $cm^2\ g^{-1}$, 1624 $cm^2\ g^{-1}$, and 1588 $cm^2\ g^{-1}$, respectively. These results are much larger than the usual specific surface area, which is between 1250–1600 $m^2\ g^{-1}$ from several synthesis methods.[25] The adsorption and desorption profiles of N_2 on Fe5-ZIF-8 shows that the material type exhibits a type 1 isotherm indicating a solid material with micropores (0.1–2.5 nm) the same as pure ZIF-8.[26,27] In addition, Rendless Sevicks approach was used to calculate the diffusion coefficient of each sample. Based on the eqn (1) where, i_p (A) is the current peak in the oxidation process, n is the total number of electrons exchanged in a redox reaction, in this case 2, A (cm^2) is electrode active area, C (mol cm^{-3}) is the concentration of the dopamine in the solution (0.1 mM), D ($cm^2\ s^{-1}$) is the diffusion coefficient and v (V s^{-1}) is the scan rate.[28]

$$i_p = 0.4463nFAC\left(\frac{nFvD}{RT}\right)^{\frac{1}{2}} = 2.69 \times 10^5 n^{3/2} ACD^{1/2} v^{1/2} \text{ at } 25\ ^\circ\text{C} \quad (1)$$

Diffusion coefficient relates to the how fast the dopamine molecule difuse to the surface of electrode and it also depends on the catalytic activity of the electrode. D value of Fe5-ZIF-8 is found to be the highest among all the samples which is 0.003 $cm^2\ s^{-1}$ including the bare GCE (0.002 $cm^2\ s^{-1}$). Consequently, further testing was carried out specifically on Fe5-ZIF-8.

The reduction–oxidation (redox) reaction mechanism of dopamine consists of two stages; the first stage involves a reversible reaction where dopamine is converted to dopamine-*o*-quinone. The second stage is an irreversible cyclization process where dopamine-*o*-quinone transforms into leukoaminochrome. The primary focus of the oxidation–reduction reactions lies in the first stage that occur on the metal center of Zn^{2+} and Fe^{2+}.[29] Fig. 4b illustrates CV measurements conducted with variations in scan rate (v), which can provide insights into the charge transfer mechanism at the electrode surface.[28] When dealing with redox species that can freely diffuse, the current response will exhibit a linear increase with the square root of the scan rate ($v^{1/2}$). Conversely, for species that are adsorbed onto the electrode surface, the current response will linearly increase with the scan rate (v). In this study, measurements were performed on 0.1 mM of dopamine (0.01 M PBS pH 7.4) at scan rates ranging from 25 mV s^{-1} to 200 mV s^{-1}. The inset plot in Fig. 4b demonstrates a linear correlation between the current magnitudes of the oxidation and reduction peaks and the scan rate. This indicates that the charge transfer in this system is diffusion-controlled.

For the assessment of the sensor's sensitivity, a DPV test was conducted by varying the concentration within the range of 0.05 μM to 20 μM and scanning from −0.05–0.3 V. The DPV peak currents corresponding to each measured concentration that can be found in Fig. 4c. The DPV curve demonstrates by analyzing the relationship between the peak current profile and concentration, sensitivity can be obtained from the slope which

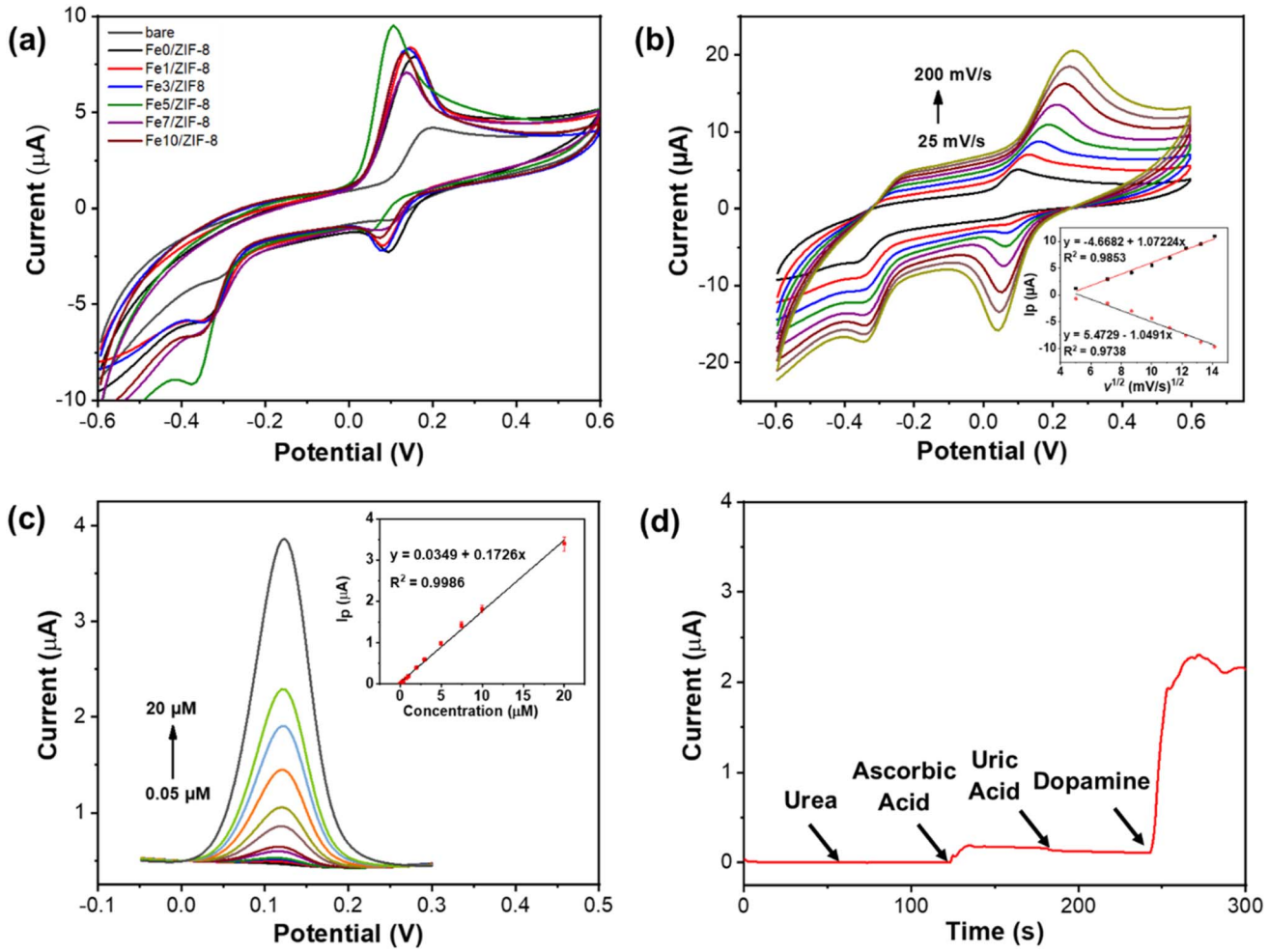

Fig. 4 (a) Cyclic Voltamogram (CV) of Fe-ZIF-8/GCE modifications including bare in 0.01 M PBS containing 0.1 mM dopamine. (b) CV of Fe5-ZIF-8/GCE at different scan rates in 0.01 M PBS containing 0.1 mM dopamine. (c) Sensitivity of Fe5-ZIF-8/GCE measured using DPV technique and its linearity. (d) Selectivity of Fe5-ZIF-8/GCE measured using chronoamperometric in 0.1 mM of dopamine, urea, ascorbic acid, and uric acid.

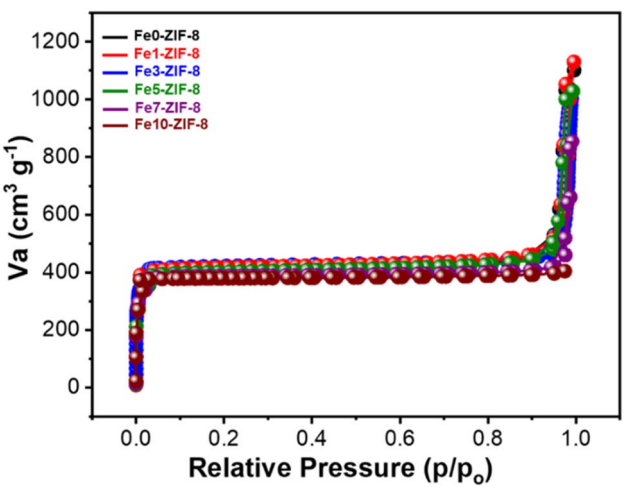

Fig. 5 N_2 adsorption desorption isotherm curves of Fe0-ZIF-8, Fe1-ZIF-8, Fe3-ZIF-8, Fe5-ZIF-8, Fe7-ZIF-8, and Fe10-ZIF-8.

is being 0.1726 μA μM^{-1}. Moreover it becomes possible to determine the limit of detection (LOD) using the following eqn (2).

$$\mathrm{LOD} = \frac{3\sigma}{m} \quad (2)$$

where the value of 3 is the signal-to-noise ratio (S/N), σ is the standard deviation and m is the slope of the linear curve. The LOD of the sensor is found to be 0.035 μM. Additionally, based on the DPV curves, it is evident that the current generated by dopamine is linear with the concentration of dopamine provided. This indicates the occurrence of an electron transfer reaction. This phenomenon is demonstrated by EIS testing with and without the presence of 0.1 mM of dopamine, as shown in Fig. 6a. Qualitatively, the charge transfer resistance decreases after the addition of dopamine. Based on EIS fitting with the equivalent circuit and the eqn (3), the charge transfer resistances with and without dopamine are 84 KΩ and 540 KΩ, respectively.[30]

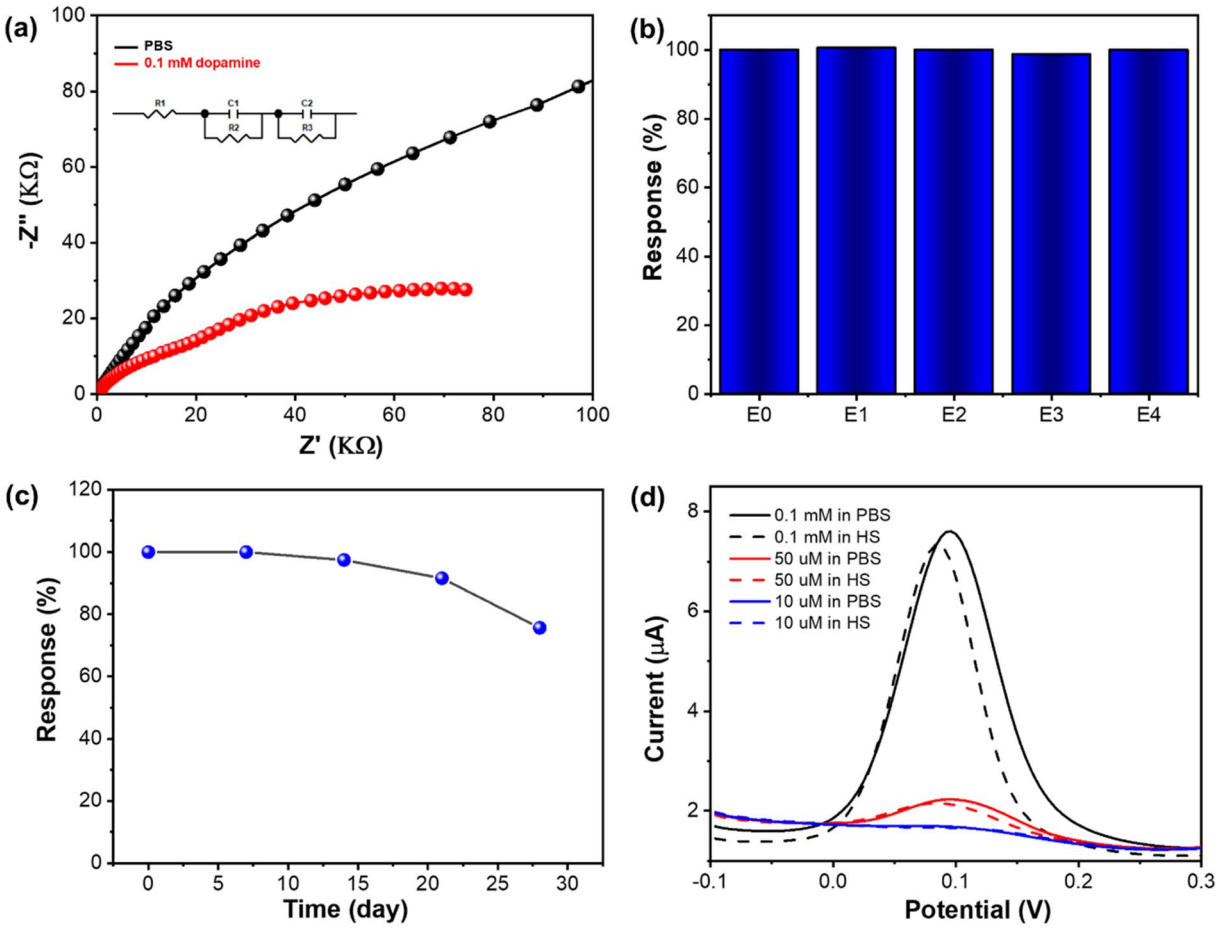

Fig. 6 (a) EIS curve of Fe5-ZIF-8 measured with and without 0.1 mM dopamine. (b) Repeatability of Fe5-ZIF-8 checked at five different electrodes. (c) And stability of Fe5-ZIF-8 for 4 weeks. (d) DPV curves response of Fe5-ZIF-8 toward 10 μM, 50 μM, and 0.1 mM of dopamine in PBS and human serum.

$$Z_{\text{total}} = R_1 + \frac{R_2}{1 + j\omega C_1 R_2} + \frac{R_3}{1 + j\omega C_2 R_3} \quad (3)$$

To determine the selectivity of the sensor, a CA test was conducted in a stirred solution at a constant potential of 0.1 V. The purpose was to observe any changes in current when potential interferences were introduced, which could potentially affect the accurate measurement of dopamine. The CA test was performed in a stirred solution containing a 0.01 M of PBS solution. At specific time intervals, different substances were

Table 1 Comparison of figures of merit on previous dopamine sensors with the present work

Electrode modification	Methods	Linear range	LOD (μM)	References
Au@PSi-P3HT	CV	1.0–460 μM	0.63	31
Carbon dots	DPV	0.25–76.81 μM	0.08	32
Carbon quantum dots (CQDs) and copper oxide (CuO) nanocomposite	CV	1–180 μM	25.4	33
Nanocomposite of graphene quantum dots (GQDs, 1–5 nm) and multiwall carbon nanotubes (MWCNTs)	DPV	0.25–250 μM	0.095	34
A three-dimensional (3D) porous carbon sheet with hierarchical ordered mesopores	DPV	0.8–400 μM	0.1	35
A platinum–silver graphene (Pt–Ag/Gr) nanocomposite	DPV	0.1–60 μM	0.012	7
Graphene oxide thin film	DPV	0–200 μM	9.3	36
Graphene oxide-UIO-66	DPV	0–200 μM	2.1	36
Binary copper selenide prepared by hydrothermal method	CA	40–640 μM	0.068	37
Binary copper selenide prepared by electrodeposition method	CA	40–320 μM	0.098	37
Fe-ZIF-8	DPV	0.05–20 μM	0.035	This work

added to the solution to create interference. Urea was added at 60 seconds, ascorbic acid at 120 seconds, uric acid at 180 seconds, and dopamine at 240 seconds. The concentrations of each substance were adjusted accordingly: urea at 10 mM, ascorbic acid at 1 mM, uric acid at 1 mM, and dopamine at 0.1 mM (see in Fig. 4d). The measurement results indicate that the dopamine electrochemical sensor utilizing Fe5-ZIF-8 material exhibits a selective response specifically towards dopamine.

Additionally, to further assess the performance of Fe5-ZIF-8 as a dopamine sensor, five different electrodes were prepared to check their consistency in term of signal after interacting with 0.1 mM of dopamine. As shown in Fig. 6b, the five electrodes generated similar response values with deviation standard of 0.05%, indicating the excellent reproducibility. Moreover, five different electrodes were also prepared to check their stability. All the electrodes were stored at room temperature and each electrode was evaluated every week for four weeks. As shown in Fig. 6c, the sensor still gives 100% of its performance after 14 days storing and decreasing to 75% at the end of 28 days. This stability is still needing further improvement. However, the electrode demonstrates similar responses when detecting dopamine in human serum compared to PBS (Fig. 6d), where the recoveries for 10 μM, 50 μM and 0.1 mM are 99%, 97%, and 95%, respectively revealing its high potential in practical use.

This modification demonstrates significant success by achieving a smaller LOD compared to several other dopamine sensors, as shown in Table 1. This table compares the results of other sensors with the findings of this study.

4. Conclusion

The synthesis of various Fe-ZIF-8 composites with different iron ratios (Fe0-ZIF-8, Fe1-ZIF-8, Fe3-ZIF-8, Fe5-ZIF-8, Fe7-ZIF-8, and Fe10-ZIF-8) was successfully achieved using a precipitation method at room temperature. The optimal iron ratio was determined based on SEM and CV analysis, which showed that Fe5-ZIF-8/GCE exhibited the highest oxidation and reduction peaks. The performance of the Fe5-ZIF-8/GCE sensor was also evaluated, demonstrating controlled diffusion of analytes to the electrode surface. DPV analysis showed two linear ranges in 0.05–20 μM. The limit of detection (LOD) for Fe5-ZIF-8/GCE was determined to be 0.035 μM with the lower range falling below the concentration of dopamine in urine. Furthermore, the sensor exhibited selectivity towards interfering substances such as uric acid, ascorbic acid, and urea. Overall, these findings highlight the successful synthesis and promising performance of Fe5-ZIF-8 as a selective sensor material.

Data availability

Data for this article are available at Science Data Bank at **https://doi.org/10.57760/sciencedb.12968**.

Conflicts of interest

There are no conflicts to declare.

Acknowledgements

This work was supported by Penelitian Pengabdian Masyarakat dan Inovasi Program managed by Institut Teknologi Bandung, Indonesia. This work was also supported by Lembaga Pengelola Dana Pendidikan (LPDP) and National Research and Innovation Agency (BRIN) under the scheme of Riset dan Inovasi untuk Indonesia Maju batch 4 (RIIM-4) No. B-3842/II.7.5/FR.06.00/11/2023 and B-3855/III.10/FR.06.00/11/2023. Authors also acknowledge the support from Nanotechnology and Material Organization Research of BRIN and Institut Teknologi Bandung, Indonesia.

References

1 H. Juárez Olguín, D. Calderón Guzmán, E. Hernández García and G. Barragán Mejía, *Oxid. Med. Cell. Longevity*, 2016, **2016**, 9730467.
2 T.-S. Wong, G. Li, S. Li, W. Gao, G. Chen, S. Gan, M. Zhang, H. Li, S. Wu and Y. Du, *Signal Transduction Targeted Ther.*, 2023, **8**, 177.
3 H. Xu and F. Yang, *Transl. Psychiatry*, 2022, **12**, 464.
4 Z.-L. Yang, H. Li, B. Wang and S.-Y. Liu, *J. Chromatogr. B*, 2016, **1012–1013**, 79–88.
5 K. K. Dewi, N. L. W. Septiani, N. Nugraha, D. Natalia and B. Yuliarto, *J. Electrochem. Soc.*, 2022, **169**, 97506.
6 M. Sajid, M. K. Nazal, M. Mansha, A. Alsharaa, S. M. S. Jillani and C. Basheer, *TrAC, Trends Anal. Chem.*, 2016, **76**, 15–29.
7 N. S. Anuar, W. J. Basirun, Md. Shalauddin and S. Akhter, *RSC Adv.*, 2020, **10**, 17336–17344.
8 S. Chelly, M. Chelly, R. Zribi, R. Gdoura, H. Bouaziz-Ketata and G. Neri, *ACS Omega*, 2021, **6**, 23666–23675.
9 S. R. Ali, R. R. Parajuli, Y. Ma, Y. Balogun and H. He, *J. Phys. Chem. B*, 2007, **111**, 12275–12281.
10 J.-M. Zen, C.-T. Hsu, Y.-L. Hsu, J.-W. Sue and E. D. Conte, *Anal. Chem.*, 2004, **76**, 4251–4255.
11 J. Cravillon, S. Münzer, S.-J. Lohmeier, A. Feldhoff, K. Huber and M. Wiebcke, *Chem. Mater.*, 2009, **21**, 1410–1412.
12 L. Cheng, P. Yan, X. Yang, H. Zou, H. Yang and H. Liang, *J. Alloys Compd.*, 2020, **825**, 154132.
13 A. Paul, I. K. Banga, S. Muthukumar and S. Prasad, *ACS Omega*, 2022, **7**, 26993–27003.
14 Z. Wang, R. Han, L. Li, J. Sun, J. Yang, M. Pan and S. Wang, *Microchem. J.*, 2023, **185**, 108286.
15 M. T. Thanh, T. V. Thien, P. D. Du, N. P. Hung and D. Q. Khieu, *J. Porous Mater.*, 2018, **25**, 857–869.
16 H. Yang, S. Hu, H. Zhao, X. Luo, Y. Liu, C. Deng, Y. Yu, T. Hu, S. Shan, Y. Zhi, H. Su and L. Jiang, *J. Hazard. Mater.*, 2021, **416**, 126046.
17 Y. Zhang, Y. Sun, Y. Man, H. Yuan, R. Zhao, G. Xiang, X. Jiang, L. He and S. Zhang, *Chem. Eng. J.*, 2022, **440**, 135723.
18 M. T. Thanh, T. V. Thien, P. D. Du, N. P. Hung and D. Q. Khieu, *J. Porous Mater.*, 2018, **25**, 857–869.
19 H. Yang, S. Hu, H. Zhao, X. Luo, Y. Liu, C. Deng, Y. Yu, T. Hu, S. Shan, Y. Zhi, H. Su and L. Jiang, *J. Hazard. Mater.*, 2021, **416**, 126046.

20 B. Zheng, Y. Zhu, F. Fu, L. L. Wang, J. Wang and H. Du, *RSC Adv.*, 2017, **7**, 41499–41503.
21 H. Kaur, G. C. Mohanta, V. Gupta, D. Kukkar and S. Tyagi, *J. Drug Delivery Sci. Technol.*, 2017, **41**, 106–112.
22 A. Schejn, L. Balan, V. Falk, L. Aranda, G. Medjahdi and R. Schneider, *CrystEngComm*, 2014, **16**, 4493–4500.
23 O. M. Linder-Patton, T. J. de Prinse, S. Furukawa, S. G. Bell, K. Sumida, C. J. Doonan and C. J. Sumby, *CrystEngComm*, 2018, **20**, 4926–4934.
24 T. Shinagawa, A. T. Garcia-Esparza and K. Takanabe, *Sci. Rep.*, 2015, **5**, 13801.
25 Y. R. Lee, M. S. Jang, H. Y. Cho, H. J. Kwon, S. Kim and W. S. Ahn, *Chem. Eng. J.*, 2015, **271**, 276–280.
26 Z. Li, X. Huang, C. Sun, X. Chen, J. Hu, A. Stein and B. Tang, *J. Mater. Sci.*, 2017, **52**, 3979–3991.
27 M. Kruk and M. Jaroniec, *Chem. Mater.*, 2001, **13**, 3169–3183.
28 K. K. Dewi, N. L. W. Septiani, S. Wustoni, Nugraha, S. N. A. Jenie, R. V. Manurung and B. Yuliarto, *ACS Omega*, 2024, **9**, 1454–1462.
29 R. P. Bacil, L. Chen, S. H. P. Serrano and R. G. Compton, *Phys. Chem. Chem. Phys.*, 2020, **22**, 607–614.
30 H. H. Hernández, A. M. R. Reynoso, J. C. T. González, C. O. G. Morán, J. G. M. Hernández, A. M. Ruiz, J. M. Hernández and R. O. Cruz, in *Electrochemical Impedance Spectroscopy*, ed. M. El-Azazy, M. Min and P. Annus, IntechOpen, Rijeka, 2020, ch. 1.
31 J. Ahmed, M. Faisal, S. A. Alsareii, M. Jalalah and F. A. Harraz, *J. Alloys Compd.*, 2023, **931**, 167403.
32 R. Wu, S. Yu, S. Chen, Y. Dang, S. H. Wen, J. Tang, Y. Zhou and J. J. Zhu, *Anal. Chim. Acta*, 2022, **1229**, 1–9.
33 S. E. Elugoke, O. E. Fayemi, A. S. Adekunle, B. B. Mamba, T. T. I. Nkambule and E. E. Ebenso, *FlatChem*, 2022, **33**, 100372.
34 S. K. Arumugasamy, S. Govindaraju and K. Yun, *Appl. Surf. Sci.*, 2020, **508**, 145294.
35 S. Wang, P. Guo, G. Ma, J. Wei, Z. Wang, L. Cui, L. Sun and A. Wang, *Electrochim. Acta*, 2020, **360**, 137016.
36 Y.-N. Chang, C.-H. Shen, C.-W. Huang, M.-D. Tsai and C.-W. Kung, *ACS Appl. Nano Mater.*, 2023, **6**, 3675–3684.
37 S. Umapathi, J. Masud, H. Coleman and M. Nath, *Microchim. Acta*, 2020, **187**, 440.